Supporting Information

Photochemical reaction pathways of carbon tetrabromide in solution probed by picosecond X-ray diffraction

Qingyu Kong,[†] Michael Wulff,[†] Jae Hyuk Lee,[§] Savo Bratos,[‡] Hyotcherl Ihee[*§]

† European Synchrotron Radiation Facility, Grenoble Cedex 38043, BP 220, France

§ National Creative Research Initiative Center for Time-Resolved Diffraction, Department of Chemistry and School of Molecular Science (BK21), Korea Advanced Institute of Science and Technology (KAIST), Daejeon, 305-701, Republic of Korea

‡ Laboratoire de Physique, Théorique des Liquides, Université Pierre et Marie Curie, Case Courrier 121, 4 Place Jussieu, Paris Cedex 75252, France

To whom correspondence should be addressed: Hyotcherl Ihee, hyotcherl.ihee@kaist.ac.kr

Global fitting analysis and kinetics of various solute molecules

The scattering intensity from a solution consists of three parts: the scattering from the solute molecule itself, the bulk solvent, and the solvent/solute cross-term (cage). The bulk solvent response to the temperature and density change caused by the reaction can be described with the temperature and density derivatives determined by impulsive heating of solvent by NIR as follows [S1]:

$$\Delta S_{solvent}(q) = \left(\frac{\partial S}{\partial T}\right)_{\rho} \Delta T + \left(\frac{\partial S}{\partial \rho}\right)_{T} \Delta\rho$$

Molecular Dynamics (MD) simulation provides the scattering intensities from solutes and solute-solvent cross-terms. Hence the total scattering intensity is composed of the sum of each scattering intensity [S2]:

$$\Delta S_{theory}(q) = \left[\sum_k f_k(t) S_k(q) - S_g(q) \sum_k f_k(0)\right] + \left(\frac{\partial S}{\partial T}\right)_{\rho} \Delta T + \left(\frac{\partial S}{\partial \rho}\right)_{T} \Delta\rho$$

where k is the index of the solute (reactant, product, and intermediates), f_k is the fraction of each molecule, $S_k(q)$ is the scattering intensity of k, and $S_g(q)$ is the scattering intensities of reactants.

To extract a reaction mechanism from these results, a reaction model including all reasonable candidate reaction pathways was used as shown in Figure S1. Based on this model, concentration changes of various chemical species with time can be calculated by integrating the following set of differential rate equations:

$$\begin{aligned}
\partial[\mathrm{CBr}_{4,parent}] &= -k_1[\mathrm{CBr}_{4,parent}] \\
\partial[\mathrm{CBr}_3] &= k_1[\mathrm{CBr}_{4,parent}] - D_1[\mathrm{CBr}_3][\mathrm{Br}] - D_2[\mathrm{CBr}_3][\mathrm{CBr}_3] \\
\partial[\mathrm{Br}] &= k_1[\mathrm{CBr}_{4,parent}] - D_1[\mathrm{CBr}_3][\mathrm{Br}] - D_3[\mathrm{Br}][\mathrm{Br}] \\
\partial[\mathrm{isomer}] &= D_1[\mathrm{CBr}_3][\mathrm{Br}] - k_3[\mathrm{isomer}] \\
\partial[\mathrm{C_2Br_6}] &= D_2[\mathrm{CBr}_3][\mathrm{CBr}_3] - k_4[\mathrm{C_2Br_6}] \\
\partial[\mathrm{C_2Br_4}] &= k_4[\mathrm{C_2Br_6}] \\
\partial[\mathrm{Br_2}] &= D_3[\mathrm{Br}][\mathrm{Br}] + k_4[\mathrm{C_2Br_6}] \\
\partial[\mathrm{CBr}_{4,final}] &= k_3[\mathrm{isomer}]
\end{aligned}$$

where $\partial[\mathrm{CBr}_{4,parent}]$, as an example, is the time derivative of the concentration change of CBr_4, *ks* are rate constants for first-order reactions, and Ds are bimolecular rate

constants. The concentration of CBr_4 is separated into two parts: the initial concentration and the newly formed concentration. Integrating the rate equations provides f_k, the fraction of each molecule, to be used to construct the theoretical diffraction signal. The strategy of the least-squares fits to the experimental data with the theoretical diffraction curve is to minimize the total χ^2 iteratively in a global-fitting procedure of simultaneously minimizing the curves at all positive time delays [S2]:

$$\chi^2 = \sum_{j=\text{time delay}} \chi_j^2$$

$$\chi_j^2 = \sum_i \left(\frac{\Delta S_{\text{theory}}(q_i, t_j) - \Delta S_{\text{experimental}}(q_i, t_j)}{\sigma_{i,j}} \right)^2$$

where $\sigma_{i,j}$ is the error bar on the experimental curves calculated as the standard deviation of the different repetitions of a given time-delay. The fitting parameters are the rate-constants. The occupancies of the respective species enter the fitting under the restriction that the number of atoms is conserved. The other fitting parameter is the laser beam size, which is used to optimize the time-constant of thermal expansion.

Hydrodynamics of the bulk solvent. As the excited CBr_4 molecule relaxes down along the potential energy surface to form the more stable C_2Br_4 and Br_2, or recoils back to the ground state through vibrational cooling, the excess energy is released as heat to the surrounding solvent. As the heat propagates through the solution, the temporal variations of the thermodynamic quantities such as the changes in density $\Delta\rho(t)$ and temperature $\Delta T(t)$ of the bulk solvent can be followed as a function of time. Figure S2 shows the temporal variations of $\Delta\rho(t)$ and $\Delta T(t)$ of the bulk solvent after laser excitation. The density decreases by 1.348 kg/m^3 at 5 μs after thermal expansion, which corresponds to a relative temperature change of 1.144 K. While the global fitting analysis provides $\Delta\rho(t)$ and $\Delta T(t)$ [S2], the same information can be extracted even without using the global fitting analysis as follows. The density change of the solution can be obtained from the sine-Fourier transforms of the measured difference diffraction intensities $\Delta S(q)$ through the following equation [S3,S4]:

$$\Delta S(r) = \frac{10^{30}}{N_A} M_{CH_3OH} \frac{1}{2\pi^2 r} \int_0^\infty \frac{q\Delta S(q)}{\sum_{i=j} f_i(q) f_j(q)} \sin(qr) e^{-(\alpha q)^2} dq$$

$$\Delta\rho = -\lim_{r\to 0} \Delta S(r)$$

where N_A is the Avogadro number, M_{CH3OH} is the mass of one methanol molecule, and $\sum_{i=j} f_i(q) f_j(q) = \sum f_i^2(q)$ is the sharpening factor. The density change as a function of time can be extracted from the small-r (r = 10/q_{max}) portion of the measured $\Delta S(r)$, while the time-dependent temperature change ($\Delta T(t)$) can be calculated via thermodynamic relations which have been described in detail by us previously [S3].

References

[S1] Cammarata, M., Lorenc, M., Kim, T. K., Lee, J. H., Kong, Q. Y., Pontecorvo, E., Lo Russo, M., Schiro, G., Cupane, A., Wulff, M.; Ihee, H. *J. Chem. Phys.* 2006, *124,* 124504.

[S2] Ihee, H.; Lorenc, M.; Kim, T. K.; Kong, Q. Y.; Cammarata, M.; Lee, J. H.; Bratos, S.; Wulff, M. *Science* 2005, *309,* 1223.

[S3] Wulff, M.; Bratos, S.; Plech, A.; Vuilleumier, R.; Mirloup, F.; Lorenc, M.; Kong, Q. Y.; Ihee, H. *J. Chem. Phys.* 2006, *124,* 034501.

[S4] Bratos, S.; Mirloup, F.; Vuilleumier, R.; Wulff, M.; Plech, A. *Chem. Phys.* 2004, *304,* 245.

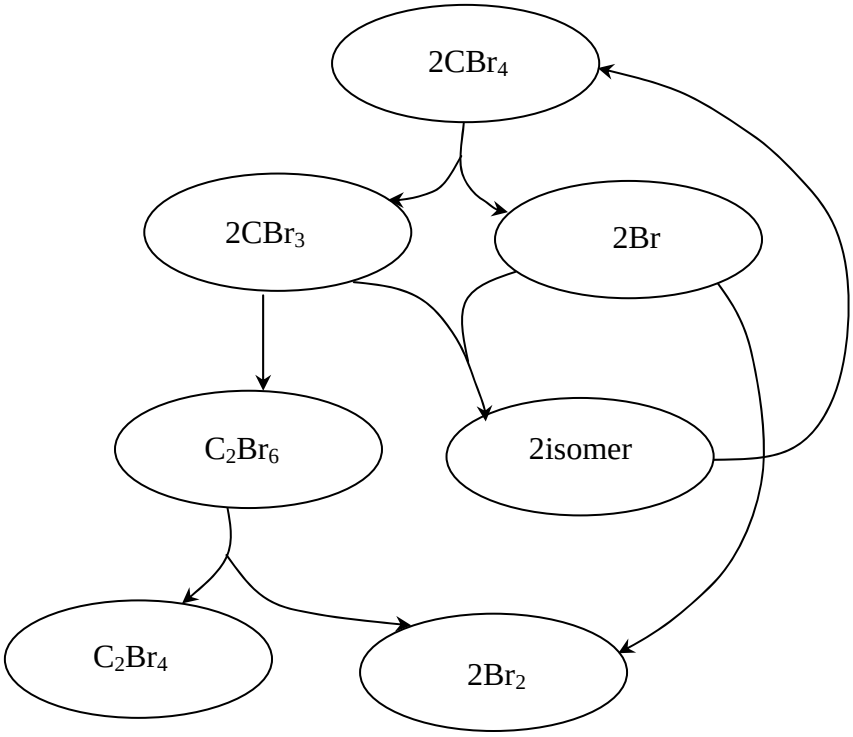

Figure S1. Schematic of the photodissociation reaction pathways for CBr_4

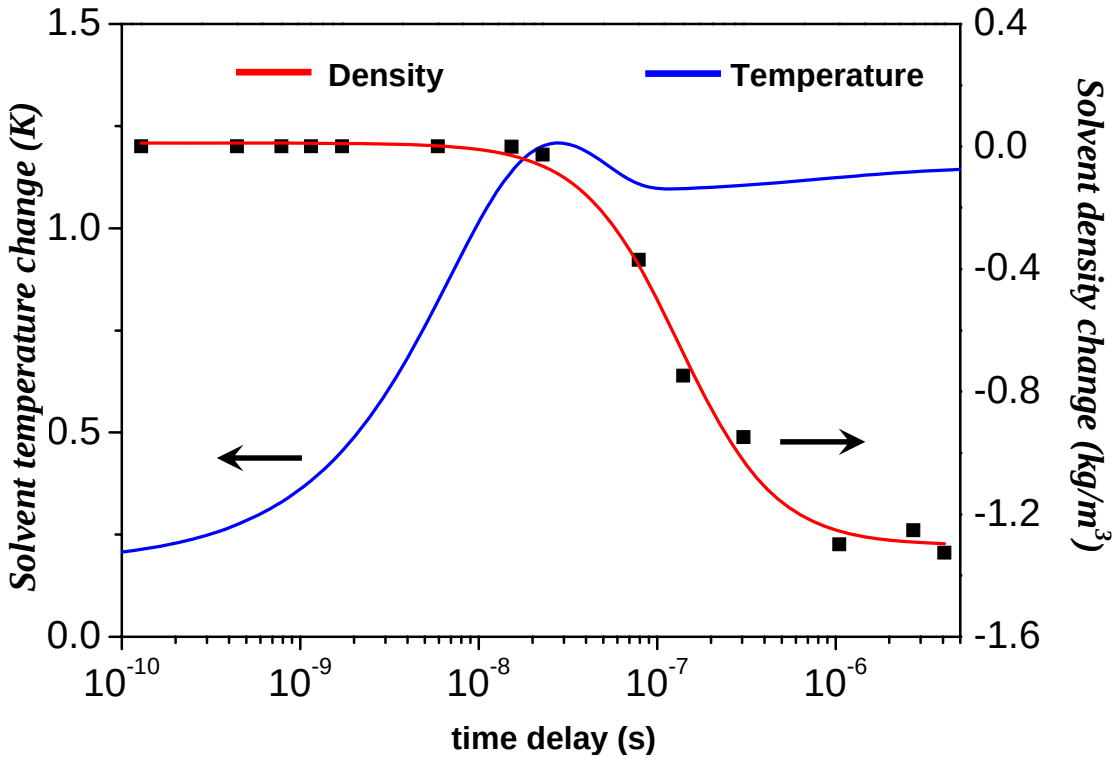

Figure S2. Temporal variations of the solvent density $\Delta\rho(t)$ and solvent temperature $\Delta T(t)$ from global fitting analysis. Arrows point to the corresponding axis for each curve. The rectangular squares were obtained from another method (see the text). Please note that the results from two deferent methods are consistent.

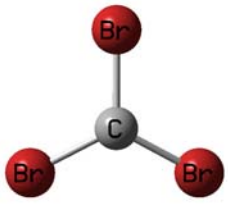

CBr_3 Umbrella
Br-Br: 3.221 Å
C-Br: 1.885 Å
∠BrCBr=117.397 degree

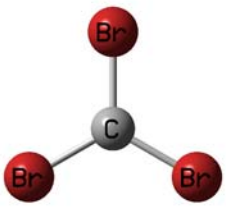

CBr_3^+ planer
Br-Br: 3.150 Å
C-Br: 1.819 Å
∠BrCBr=120.0 degree

Figure S3. Geometry of CBr_3 and CBr_3^+ in methanol from a density functional theory (DFT) calculation, at B3LYP/6-311+G(3df) level. The SCIPCM model is used to include the solvent effect.

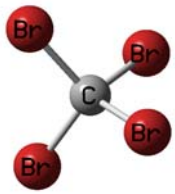

CBr_4 ^1A_g
C-Br: 1.957 Å
Br-Br: 3.196 Å

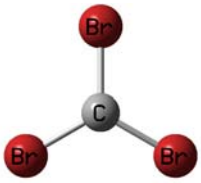

CBr_3 $^2A_1$
Br-Br: 3.221 Å
C-Br: 1.885 Å

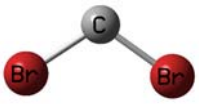

CBr_2 $^1A_1$
C-Br: 1.894 Å
Br-Br: 3.120 Å

Br_2 $^1\sum_g$
Br-Br: 2.316 Å

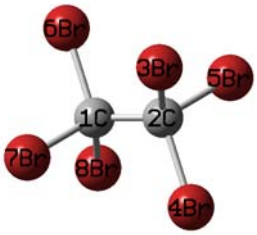

C_2Br_6 $^1A_{1g}$
C-C: 1.569 Å
1C-6Br: 1.966 Å
1C-3Br: 2.920 Å
3Br-5Br: 3.183 Å
3Br-6Br: 3.493 Å
6Br-4Br: 4.725 Å

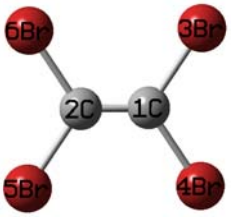

C_2Br_4 ^1A_g
C-C: 1.336 Å
1C-3Br: 1.892 Å
1C-6Br: 2.849 Å
3Br-4Br: 3.175 Å
3Br-6Br: 3.395 Å
3Br-5Br: 4.648 Å

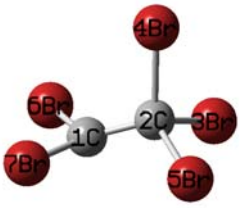

C_2Br_5 $^2A'$
C-C: 1.473 Å
1C-6Br: 1.874 Å
1C-5Br: 2.866 Å
1C-4Br: 2.889 Å
6Br-7Br: 3.169 Å
6Br-4Br: 3.842 Å
6Br-5Br: 4.639 Å
6Br-3Br: 3.388 Å
4Br-3Br: 3.231 Å
3Br-5Br: 3.170 Å

CBr_3-Br isomer $^1A'$
1C-4Br: 1.844 Å
1C-2Br: 1.851 Å
1C-3Br: 4.628 Å
2Br-3Br: 2.849 Å
2Br-4Br: 3.210 Å
4Br-5Br: 3.161 Å
3Br-4Br: 5.746 Å

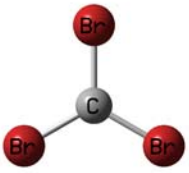

CBr_3^+ $^1A_1$
Br-Br: 3.150 Å
C-Br: 1.819 Å

Figure S4. Geometries and bond lengths of various molecules CBr_4, CBr_3, CBr_2, Br_2, C_2Br_6, C_2Br_4, CBr_3-Br isomer, CBr_3^+ and C_2Br_5 in methanol used in the data analysis. The geometries were calculated with DFT at the B3LYP/6-311+G(3df) level. The SCIPCM model was used to include the solvent effect.

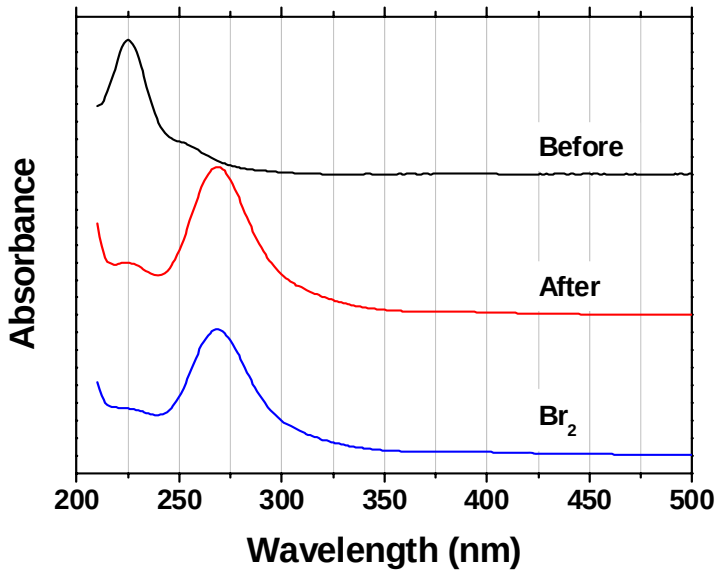

Figure S5. UV/VIS spectra before and after photolysis at 266 nm. A CBr_4 in methanol solution at 5 mM was irradiated at 267 nm with nanosecond pulses with the sample being stirred. The top spectrum is the sample before irradiation and the middle spectrum is the sample after irradiation. The bottom spectrum is from the solution of Br_2 dissolved in methanol. The spectrum after photolysis clearly shows new absorption due to Br_2.

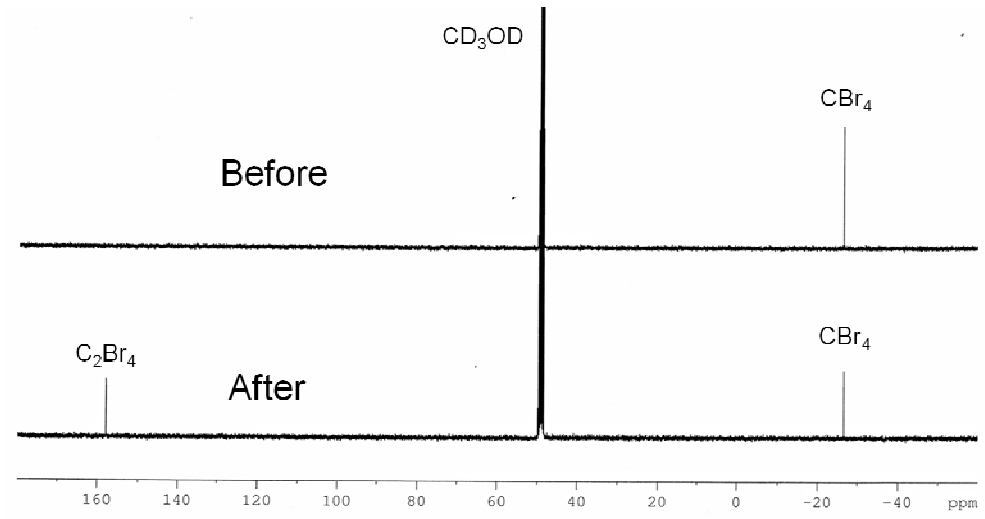

Figure S6. ^{13}C NMR spectra before and after photolysis at 266 nm. A $^{13}CBr_4$ in CD_3OD at 5 mM was irradiated at 266 nm with nanosecond pulses with the sample being stirred. The irradiated sample shows a new peak at 158 ppm which is characteristic of double bond for C_2Br_4. There are no other new peaks, meaning that C_2Br_4 is the only carbon-containing final photoproduct.

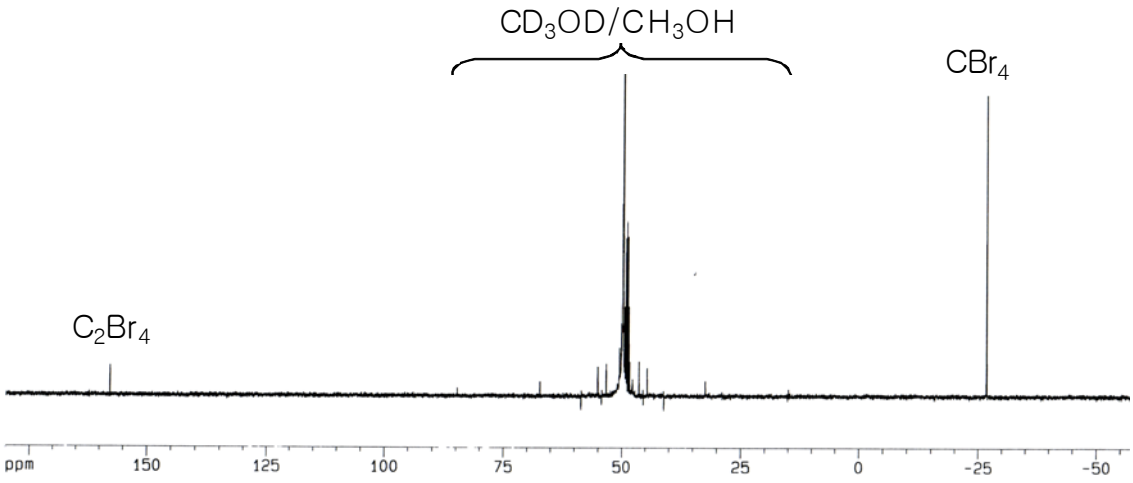

Figure S7. ^{13}C NMR spectrrum after photolysis at 266 nm. A $^{13}CBr_4$ in methanol solution (90% CH_3OH and 10% CD_3OD) at 5 mM was irradiated at 266 nm with nanosecond pulses with the sample being stirred. The irradiated sample shows a new peak at 158 ppm which is characteristic of double bond for C_2Br_4. There are no other new peaks, meaning that C_2Br_4 is the only carbon-containing photoproduct.

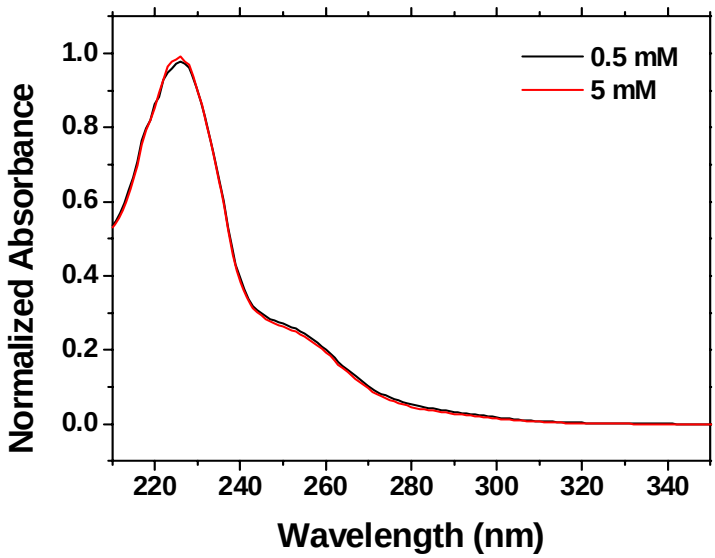

Figure S8. UV/VIS spectra of CBr_4 in methanol solution at 0.5 mM and 5 mM concentrations. They are scaled and overlaid. The absorption does not depend significantly on concentration, implying that the aggregation is negligible in the studied concentration range.

Complete citation for reference 19

Ref (19) Frisch, M. J.; Trucks, G. W.; Schlegel, H. B.; Scuseria, G. E.; Robb, M. A.; Cheeseman, J. R.; Montgomery, Jr., J. A.; Vreven, T.; Kudin, K. N.; Burant, J. C.; Millam, J. M.; Iyengar, S. S.; Tomasi, J.; Barone, V.; Mennucci, B.; Cossi, M.; Scalmani, G.; Rega, N.; Petersson, G. A.; Nakatsuji, H.; Hada, M.; Ehara, M.; Toyota, K.; Fukuda, R.; Hasegawa, J.; Ishida, M.; Nakajima, T.; Honda, Y.; Kitao, O.; Nakai, H.; Klene, M.; Li, X.; Knox, J. E.; Hratchian, H. P.; Cross, J. B.; Bakken, V.; Adamo, C.; Jaramillo, J.; Gomperts, R.; Stratmann, R. E.; Yazyev, O.; Austin, A. J.; Cammi, R.; Pomelli, C.; Ochterski, J. W.; Ayala, P. Y.; Morokuma, K.; Voth, G. A.; Salvador, P.; Dannenberg, J. J.; Zakrzewski, V. G.; Dapprich, S.; Daniels, A. D.; Strain, M. C.; Farkas, O.; Malick, D. K.; Rabuck, A. D.; Raghavachari, K.; Foresman, J. B.; Ortiz, J. V.; Cui, Q.; Baboul, A. G.; Clifford, S.; Cioslowski, J.; Stefanov, B. B.; Liu, G.; Liashenko, A.; Piskorz, P.; Komaromi, I.; Martin, R. L.; Fox, D. J.; Keith, T.; Al-Laham, M. A.; Peng, C. Y.; Nanayakkara, A.; Challacombe, M.; Gill, P. M. W.; Johnson, B.; Chen, W.; Wong, M. W.; Gonzalez, C.; Pople, J. A. Gaussian 03, Revision C.02; Gaussian, Inc.: Wallingford, CT, 2004.